Inorganic Chemistry

Article

pubs.acs.org/IC

Multiple, Disparate Redox Pathways Exhibited by a Tris(pyrrolido)ethane Iron Complex

Graham T. Sazama and Theodore A. Betley*

Department of Chemistry and Chemical Biology, Harvard University, 12 Oxford Street, Cambridge, Massachusetts 02138, United States

Supporting Information

ABSTRACT: Iron(III) complexes of the tris(pyrrolide)-ethane trianion have been synthesized by reaction of one- and two-electron oxidants with [(tpe)Fe(THF)][Li(THF)$_4$] (tpe = tris(5-mesitylpyrrolyl)ethane). X-ray crystallography, ^{57}Fe Mössbauer, ^{1}H NMR and EPR spectroscopy, SQUID magnetometry, and density functional theory calculations were employed to rigorously establish the iron 3+ oxidation state. All oxidants employed are proposed to operate via an inner-sphere electron transfer mechanism. Dialkyl peroxides and dibenzyldisulfide served to oxidize iron by one electron, and group transfer of an aryl nitrene unit to the Fe^{2+} starting material resulted in formation of Fe^{3+} amido species following H-atom abstraction by a presumed nitrenoid intermediate. Single electron transfer to and from diphenyldiazoalkane was also observed to yield a diphenyldiazomethanyl radical anion antiferromagnetically coupled to the $S = 5/2$ Fe^{3+}. Isolation of Fe^{3+} complexes of tpe, in comparison with previous results wherein the tpe ligand was the redox active moiety, presents an unusual juxtaposition of two noncommunicating redox reservoirs, each accessible via different reaction pathways (namely, inner- and outer-sphere electron transfer).

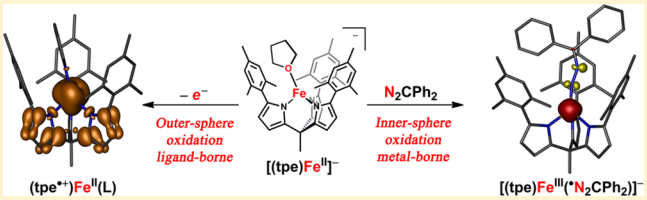

I. INTRODUCTION

Coordination complex-mediated redox chemistry involves the addition or removal of electrons from energetically accessible molecular orbitals. The bedrock of this discipline was established in the pioneering work by Taube and co-workers in the 1950s with the distinction between inner-sphere and outer-sphere electron transfer reactions.[1] In the 60 intervening years, these two mechanisms continue to be satisfactory to describe the majority of redox behavior, but many developments have been made with regards to what molecular components are involved in redox chemistry. The suite of available redox-active moieties has been expanded from simple one-electron transfers to and from transition metals to include all the fragments of a given coordination complex, including the ligands and between metals in multinuclear complexes. Molecular redox generally falls into one of the following categories described below (Scheme 1), distinguished by the redox-active fragment(s).

Type A. *Metal-Localized Redox with Redox-Inert Ligands (Scheme 1a).* In this class, all oxidation and reduction events are localized on the transition metal, suggesting a large separation between transition metal and ligand-based frontier orbitals. For type A complexes, changes in the d-orbital manifold of a given complex are readily observed spectroscopically and thus were some of the first examples of well understood redox chemistry. Redox chemistry at the metal center can simply involve the gain or loss of electrons by outer-sphere or inner-sphere mechanisms.[1] The prototypical example of this latter category is illustrated by outer-sphere oxidation of the classic Werner complex $[Co(NH_3)_6]^{2+}$(Scheme 1a).[2] As illustrated by the following examples (types A–C), care must be taken to correlate formal redox assignment to spectroscopic measurements; otherwise, type A reactivity (transition metal-centered) may be invoked inappropriately when possible ligand redox is neglected.[3]

Type B. *Ligand-Localized Redox with Redox-Inert Metals (Scheme 1b).* When the frontier orbitals of the coordination complex ligands are of sufficiently high energy (described as redox noninnocent), redox equivalents can be derived from both transition metal centers and the ligands themselves.[4] Type B complexes concern coordination complexes where redox equivalents are predominantly localized on a ligand with minimal metal character contributing to the electroactive molecular orbital(s).[5] The earliest examples of type B complexes include complexes of dithiolene ligands that may bind metals as closed-shell dianionic chelates or radical monoanionic chelates.[6] Traversing an electron transfer series with Ni induces sequential ligand oxidations without a redox change of the bound Ni (Scheme 1b). The energetically high-lying dithiolate ligand π-electrons are accessible in this sequence of redox reactions and largely comprise the redox-accessible electron reservoir for their corresponding coordination complexes. Other common chelating ligands with delocalized π-electron systems (catecholates,[7] phenolate,[8] amido-phenolate,[3,9] polyphenolateamines,[10] dianilidoamido,[11]

Received: August 29, 2013
Published: December 9, 2013

dx.doi.org/10.1021/ic402210j | Inorg. Chem. 2014, 53, 269–281

Scheme 1. Classification of Redox Behavior by Redox Localization

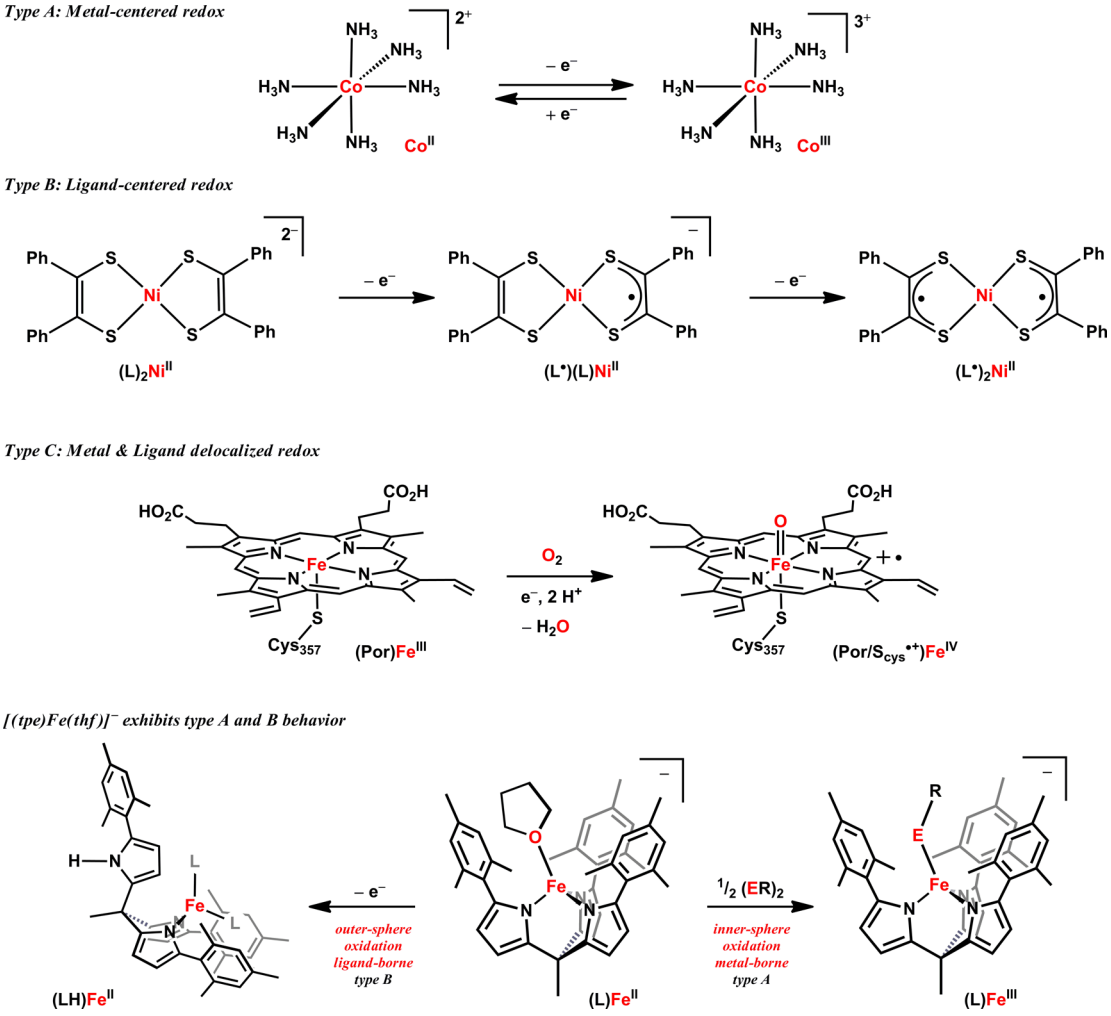

diimine,[12] diimino-pyridine,[13] imino-pyridine,[14] pyridylpyrrolides,[15] and azadipyridine[16]) have been shown to display similar, though not limited to, ligand-based redox behavior typical of type B coordination compounds. Recent work employing redox-neutral, d^0 tantalum bound to bis(phenoxide)-amide ligands extends the use of redox-active ligands from stabilization of metal centers to chemical function, wherein the complexes undergo multielectron processes with no observable change in the oxidation state of the bound metals.[17] Other examples exist which use non-d^0 transition metals bound to redox-active ligands to catalyze useful chemical transformations.[18]

Type C. *Redox Delocalized over Metal and Ligand(s) (Scheme 1c).* Redox activity need not be exclusively transition metal mediated or ligand-borne, as multielectron redox processes can be effected wherein multiple redox equivalents are stored on both the metal and the ligand. Successive redox events occur in the highest energy molecular orbitals, regardless of whether the orbitals are localized on the metal or ligand or delocalized across the whole molecule. Cytochrome P-450 is the paradigm for type C coordination complexes.[19,20] Initial binding of dioxygen oxidizes iron from the 2+ to the 3+ oxidation state. Upon O−O bond scission, two oxidizing equivalents are transferred: one oxidizes iron to the 4+ state, and the other is delocalized about the porpyhrin ligand[21] and the proximal cysteine thiolate (Scheme 1c).[22] This type of ligand and transition metal distributed redox reactivity is expressed most simply as molecular redox states, wherein the location of oxidation state changes are not assigned. Other coordination complexes that display significant ligand−metal redox interplay include complexes utilizing corroles,[23] porphyrinogens,[24] diiminopyridines,[25] iminopyridines,[18c] diimines,[26] aminophenolates,[27] and catechol species.[28]

In the pursuit of type C compounds, we have discovered a complex that exhibits both type A and B behavior dependent upon the reaction mechanism: outer-sphere electrochemical or chemical electron transfer results in ligand-borne oxidation (type B); whereas inner-sphere oxidation mediated by coordinating oxidants oxidizes the complexes locally at the metal (type A). The synthesis and characterization of these materials and a proposed mechanism for the latter type of reactivity are presented here. In addition, an iron diazoalkane complex is synthesized and characterized, resulting in a complex intermediate between the limiting resonance structures of a bound neutral diazoalkane adduct and a doubly reduced adduct exhibiting imido-like properties.

We previously reported the outer-sphere oxidation of a series of $[(tpe)M^{2+}(py)]^-$ complexes (M = Mn, Fe, Co, Ni, Zn) via electrochemical or chemical methods (tpe = tris(5-mesitylpyrrolyl)ethane).[29] Examination of the electrochemical behavior of this series of complexes showed a common irreversible oxidative process (−655 mV vs $[Cp_2Fe]^{+/0}$) that we

dx.doi.org/10.1021/ic402210j | Inorg. Chem. 2014, 53, 269−281

proposed is ligand-based and unaffected by the identity of the bound transition metal. We attributed the observed oxidation process to removal of an electron from a tpe-derived pyrrolide π-orbital. The ligand pyrrollic π-electrons were shown to be highest in energy for the coordination complexes by density functional theory (DFT) analysis akin to their dipyrromethane analogues.[30] Further inspection of the DFT and electrochemical results reveals a seemingly non-Aufbau arrangement of electrons, resulting in a population of fully filled, delocalized ligand π-orbitals higher in energy than partially filled metal 3d orbitals. This can be attributed to a combination of larger electron-pairing energy costs for the electrons in the metal−ion 3d orbitals and a lack of orbital overlap between the highest energy pyrrolide-based orbitals and metal orbitals of the appropriate symmetry, which prevents metal and ligand delocalized molecular orbitals from forming. As a result of this orbital isolation between transition metal ion and tpe ligand, oxidation is localized on the more energetically accessible pyrrolide units of the tpe ligand. Chemical oxidation of the Zn- and Fe-bound species provided evidence for ligand oxidation, wherein a pyrrolide radical is formed leading to pyrrole dissociation and H-atom abstraction to result in a $[(\kappa^2\text{-tpeH})\text{Fe}(\text{py})_2]$ product. Furthermore, attempts to metalate the tpe ligand with Fe^{III} starting materials (i.e., FeCl_3 and base, $\text{Fe}^{\text{III}}(\text{N}(\text{SiMe}_3)_2)_3$) resulted in outer-sphere electron transfer to the Fe moiety to produce only $[(\kappa^2\text{-tpeH})\text{Fe}(\text{py})_2]$. In light of this observed oxidative instability, we wanted to investigate if the tpe construct was incompatible with higher valent states of the bound transition metal.

We present here our findings that although outer-sphere oxidation is ligand-borne, inner-sphere electron transfer reactions of the $[(\text{tpe})\text{Fe}(\text{THF})]^-$ anion result in metal-centered oxidation. The reaction of one- and two-electron oxidants with $[(\text{tpe})\text{Fe}(\text{THF})]^-$ form stable complexes which are spectroscopically revealed to contain a singly oxidized iron for both one- and two-electron oxidants. The reversible, one-electron reduction of a diazoalkane ligand by $[(\text{tpe})\text{Fe}(\text{THF})]^-$ is also observed to give a product containing a high-spin Fe^{3+} center antiferromagnetically coupled to a diazoalkane-borne radical. Each reaction demonstrates the viability of metal-centered redox activity on a ligand platform known to be redox unstable, qualifying the $[(\text{tpe})\text{Fe}]^-$ construct as a coordination complex exhibiting both type A and B behavior.

II. EXPERIMENTAL SECTION

All manipulations were carried out in the absence of water and dioxygen using standard Schlenk techniques or in an MBraun inert atmosphere drybox under a dinitrogen atmosphere. All glassware was oven-dried for a minimum of 1 h and cooled in an evacuated antechamber prior to use in the drybox. Benzene, diethyl ether, *n*-hexane, tetrahydrofuran, and toluene were dried and deoxygenated on a Glass Contour System (SG Water USA, Nashua, NH) and stored over 4 Å molecular sieves (Strem) prior to use. Benzene-d_6 (Cambridge Isotope Labs),*m*-xylene, 12-crown-4, and bis(trimethyl)-silyl ether (Sigma-Aldrich) were degassed and stored over 4 Å molecular sieves prior to use. Di-*tert*-butyl peroxide, dicumyl peroxide, and dibenzyl disulfide were purchased from Aldrich and used as received. Anhydrous iron(II) chloride was purchased from Strem and used as received. Diphenyldiazomethane,[31] mesityl azide (2,4,6-$\text{Me}_3\text{C}_6\text{H}_2\text{N}_3$),[32] 4-$^t\text{BuC}_6\text{H}_4\text{N}_3$,[33] and **1**[34] were synthesized according to published procedures. Celite 545 (J. T. Baker) and 4 Å molecular sieves were dried in either a Schlenk flask or a vacuum oven for 24 h under dynamic vacuum while heating to at least 150 °C.

Characterization and Physical Measurements. ^{1}H and ^{13}C NMR spectra were recorded on Varian Mercury 400 MHz or Varian Unity/Inova 500 MHz spectrometers. ^{1}H chemical shifts are reported relative to residual solvent peaks as reference. Elemental analyses were carried out at Complete Analysis Labs, Inc. (Parsippany, NJ).

^{57}Fe Mössbauer spectra were measured with a constant acceleration spectrometer (SEE Co., Minneapolis, MN). Isomer shifts are quoted relative to Fe foil at room temperature. Data was analyzed and simulated with Igor Pro 6 software (WaveMetrics, Portland, OR) using Lorentzian fitting functions.

EPR spectra were obtained on a Bruker EleXsys E-500 CW-EPR spectrometer. All EPR samples were crystalline samples, washed 3 times with ∼5 mL hexanes, and dissolved in ∼0.5 mL toluene, affording 0.5−2 mM solutions. Spectra were measured as frozen toluene glasses at nonsaturating microwave powers of 0.6325−2 mW. The signals from the desired material could be distinguished from contaminant radical species by acquiring variable-power spectra. The signal from impurities saturates at a much lower microwave power, allowing the two species to be distinguished.

SQUID magnetometry was carried out using a Quantum Design MPMS-5S SQUID magnetometer. Measurements were obtained using material that was recrystallized from diethyl ether by addition of trace amounts of THF and cooling to −35 °C. Under a dry nitrogen atmosphere, the microcrystalline materials obtained were finely ground and packed in a polycarbonate capsule. Warm liquid eicosane was added to suspend the material in solid wax after cooling. DC susceptibility measurements were collected in the temperature range of 5−300 K in 5 degree increments under a DC field of 5000 or 10 000 Oe. DC magnetization measurements were obtained in the temperature range of 1.8−10 K, under DC fields of 10, 20, 30, 40, 50, 60, and 70 kOe. The data collected were corrected for any diamagnetic contributions by comparison to an eicosane/capsule blank and by the application of Pascal's constants to account for any core diamagnetism.[35] The reduced magnetization data were fit using the ANISOFIT package,[36] using a range of possible spin states (S = 3/2, 2, 5/2, and 3). Reasonable fitting parameter values were only obtained for the cases in which the spin state was set as S = 2.

X-ray Crystallography. Crystal structures of **2**−**8** were collected at 100 K. Data was collected as a series of φ and/or ω scans. Data was integrated using SAINT (Bruker AXS) and scaled with a multiscan absorption correction using SADABS (Bruker AXS).[37] The structures were solved by direct methods or Patterson maps using SHELXS-97[38] and refined against F^2 on all data by full matrix least-squares with SHELXL-97. All non-hydrogen atoms were refined anisotropically. Hydrogen atoms were placed at idealized positions and refined using a riding model. The isotropic displacement parameters of all hydrogen atoms were fixed to 1.2 times the U value of the atoms they are linked to (1.5 times for methyl groups). Lithium countercations were bound by diethyl ether or THF molecules and generally showed some amount of disorder, which was treated using a disordered model and restraints and constraints as necessary. Further details on several structures are noted in the compiled CIF file (Supporting Information). Notes on **5**: the structure of **5** contains six molecules of $[(\text{tpe})\text{Fe}(\text{NHC}_6\text{H}_4{}^t\text{Bu})][\text{Li}(\text{THF})_4]$ in the asymmetric unit. The model was refined by separating the atom list into four equal sized parts and employing the BLOC command. The anilido hydrogen atoms were located in the difference map for all six molecules of the compound and were refined using a riding model thereafter. Notes on **6**: the structure of **6** was determined from data collected using a microcrystal sample and employing synchrotron radiation at the Argonne National Laboratory Advance Photon Source, ChemMatCARS.[39] The hydrogen atom residing on the anilido nitrogen was located as a Q peak in the difference map, and then refined using a riding model. Notes on **7**: the structure of **7** contains two molecules of $[(\text{tpe})\text{Fe}(\text{N}_2\text{CPh}_2)][\text{Li}(\text{L})_4]$ in the asymmetric unit. One of the molecules shows positional disorder of the tpe mesityl units and thus was refined using a disordered model.

*[(tpe)Fe(O^{t}Bu)][Li(THF)$_4$] (**2**).* A yellow-brown benzene solution (2 mL) of **1** (42.6 mg, 0.043 mmol) was added to a stirring benzene solution (1 mL) of di-*tert*-butyl peroxide (12.5 mg, 0..85 mmol) at room temperature and stirred. After approximately 2.5 h, the solution turned a deep red. ^{1}H NMR monitoring of the reaction reveals

dx.doi.org/10.1021/ic402210j | Inorg. Chem. 2014, 53, 269−281

disappearance of the peaks attributable to starting material **1** with the production of an NMR silent product. After 16 h, the solution was frozen and lyophilized and the residue was rinsed with cold hexanes to remove excess oxidant. The residue was extracted with diethyl ether. To assess yield accurately, the material can be precipitated from diethyl ether with added 12-crown-4 or diglyme at −35 °C, collected on a fritted glass funnel and washed with hexanes, affording 38.8 mg (86%) of dark red powder. If X-ray diffraction quality crystals are desired, crystals can be grown from saturated hexane solutions by avoiding crown ether, and instead extracting the residue into hexane and allowing the solution to stand at room temperature. However, these crystals are not of sufficient quality to obtain high-quality X-ray crystallographic data, and the data obtained are useful only for connectivity. Alternatively, analytically pure material can be obtained (as purple crystallites) by cooling concentrated diethyl ether solutions from room temperature to −35 °C. Comb. Anal. for the species containing THF bound lithium, $[C_{61}H_{83}FeLiN_3O_5]$ Calcd: C, 73.16; H, 8.36; N, 4.20. Found: C, 72.89; H, 8.08; N, 4.30.

[(tpe)Fe(OC(Ph)Me$_2$)][Li(THF)$_4$] (**3**). A yellow-brown benzene solution (1.5 mL) of **1** (35.1 mg, 0.035 mmol) was added to a stirring benzene solution (1 mL) of dicumyl peroxide (5.7 mg, 0.021 mmol) at room temperature and stirred. After about 3 h, the material began to color noticeably to a brown hue, and after about 6 h the solution was a deep red-brown. ^{1}H NMR monitoring of the reaction reveals disappearance of the peaks attributable to starting material **1** with the production of an NMR silent product. After 12 h, the solution was frozen and lyophilized. To assess the reaction yield, the residue was extracted into diethyl ether, and [(tpe)Fe(OC(Ph)Me$_2$)][Li(12-C-4)$_2$] was precipitated from diethyl ether at −35 °C by the addition of 12-crown-4. The resultant dark red powder was collected on a glass fritted funnel, washed with hexanes, and dried to yield 37.9 mg product (90%). Crystals suitable for X-ray diffraction can be grown by extracting the reaction product (from lyophilization) into minimal diethyl ether and cooled from room temperature to −35 °C, affording red-purple needles. Comb. Anal. for the species containing THF bound lithium cation, $[C_{66}H_{85}FeLiN_3O_5]$ Calcd: C, 74.53; H, 8.06; N, 3.95. Found: C, 74.29; H, 7.95; N, 4.01.

[(tpe)Fe(SBn)][Li(THF)$_4$] (**4**). A yellow-brown benzene solution (2 mL) of **1** (35.4 mg, 0.0354 mmol) was added to a stirring benzene solution (1 mL) of dibenzyl disulfide (4.7 mg, 0.019 mmol) at room temperature and stirred for 92 h, during which the solution turned a deep brown-purple. ^{1}H NMR monitoring of the reaction reveals disappearance of the peaks attributable to starting material **1** with the production of an NMR silent product. The solution was frozen and lyophilized. The residue was triturated with bis-trimethylsilyl ether (2 mL) and hexane (2 mL) and was recrystallized from diethyl ether at −35 °C, affording 23.3 mg (63%) of purple needles. Crystals suitable for X-ray diffraction can be grown from concentrated diethyl ether solutions cooled from room temperature to −35 °C. Comb. Anal. for $[C_{64}H_{81}FeLiN_3O_4S]$ Calcd: C, 73.10; H, 7.77; N, 4.00. Found: C, 72.84; H, 7.51; N, 4.11.

[(tpe)Fe(NHC$_6$H$_4$-4-^{t}Bu)][Li(THF)$_4$] (**5**). A yellow-brown benzene solution (2 mL) of **1** (36.0 mg, 0.0360 mmol) was added to a stirring benzene solution (2 mL) of 4-^{t}BuC$_6$H$_4$N$_3$ (7.1 mg, 0.041 mmol) at room temperature and stirred for 15 min, during which the solution turned vibrant dark purple. ^{1}H NMR monitoring of the reaction reveals disappearance of the peaks attributable to starting material **1** with the production of an NMR silent product. Volatiles were removed from an aliquant, which was submitted for IR analysis (KBr), revealing consumption of azide via disappearance of the azide stretch (υ_{N3}). Volatiles were removed in vacuo, and the resultant residue was washed with hexane (3 × 2 mL), dissolved in diethyl ether, and recrystallized by cooling the solution from room temperature to −35 °C. Crystals suitable for X-ray diffraction can be grown in concentrated diethyl ether cooled from room temperature to −35 °C. Comb. Anal. for species with THF bound Li$^+$, $[C_{67}H_{88}FeLiN_4O_4]$ Calcd: C, 74.74; H, 8.25; N, 5.21. Found: C, 74.42; H, 8.09; N, 4.99.

[(tpe)Fe(NHMes)][Li(THF)$_4$] (**6**). A benzene solution (1 mL) of 2,4,6-trimethylphenyl azide (15.7 mg, 0.095 mmol) was added to a stirring, yellow-brown benzene solution (2 mL) of **1** (80.0 mg, 0.080 mmol) at room temperature, and the solution was stirred for 15 min, during which the solution turned vibrant dark purple. ^{1}H NMR monitoring of the reaction reveals disappearance of the peaks attributable to starting material **1** with the production of an NMR silent product. Volatiles were removed from an aliquant, which was submitted for IR analysis (KBr), revealing consumption of azide via disappearance of the azide stretch (υ_{N3}). Volatiles were removed in vacuo and the resultant residue was washed with hexane (3 × 2 mL), dissolved in diethyl ether and recrystallized by cooling the solution from room temperature to −35 °C. Microcrystals suitable for X-ray diffraction with synchrotron radiation can be grown from concentrated diethyl ether solutions cooled from room temperature to −35 °C. Comb. Anal. for $[Li(THF)_4]^+$ containing species, $[C_{67}H_{88}FeLiN_4O_4]$ Calcd: C, 74.60; H, 8.16; N, 5.28. Found: C, 74.42; H, 8.09; N, 4.99.

[(tpe)Fe(N$_2$CPh$_2$)][Li(THF)$_4$] (**7**). A yellow-brown benzene solution (2 mL) of **1** (38.8 mg, 0.039 mmol) was added to a stirring benzene solution (1 mL) of diphenyldiazomethane (8.1 mg, 0.042 mmol) at room temperature, and the solution was stirred for 2.5 h, during which the solution turned a deep greenish brown. ^{1}H NMR monitoring of the reaction reveals disappearance of the peaks attributable to starting material **1** with the appearance of a new paramagnetically shifted ^{1}H NMR spectrum. IR analysis revealed a disappearance of the diazoalkane ($\upsilon_{N=N}$) stretching frequency. The solution was frozen and lyophilized. The residue was extracted into diethyl ether and crystallized by addition of a drop of THF and cooling to −35 °C, affording green plates. Crystals suitable for X-ray diffraction can be grown by addition of two drops of THF to a solution of crystallized product in *m*-xylenes and cooling to −35 °C. The product crystallizes with a large amount of solvent disorder about the lithium cations, ranging in formulation from $[Li(THF)(OEt_2)_2]^+$ to $[Li(THF)_3(OEt_2)]^+$. Analytically pure material containing the $[Li(THF)_4]^+$ cation can be obtained by precipitation of the material from a diethyl ether solution by addition of a drop of THF, cooling to −35 °C, isolation on a frit, washing with hexanes (2 mL) and drying by passing dry nitrogen through the material on the frit. ^{1}H NMR (500 MHz, C_6D_6): δ/ppm: 98.23 (br s), 55.49 (br s), 48.24 (br s), 39.95 (s), 27.94 (s), 10.56 (br s), 7.70 (s), 7.35 (s), 7.02 (s), 3.82 (br s), 2.19 (m), 1.59 (br s), 0.82 (br s), −5.32 (br s), −90.2 (br s). Comb. Anal. for $[C_{70}H_{84}FeLiN_5O_4]$ Calcd: C, 74.89; H, 7.55; N, 6.24. Found: C, 74.79; H, 7.36; N, 6.27.

[(tpe)Fe(PMe$_3$)][Li(THF)$_4$] (**8**). One drop of trimethylphosphine (PMe_3, excess) was added to a stirring, yellow-brown THF (2 mL) solution of **1** (52.3 mg, 0.052 mmol, assuming $[Li(THF)_4]^+$ as solvated cation) at room temperature and stirred for 10 min. Volatiles were removed in vacuo, and the resultant residue was dissolved in diethyl ether. A yellow-brown solid was precipitated by the addition of two drops of THF and cooling the solution to −35 °C. The precipitate was collected on a medium porosity frit, washed with 5 mL of pentane, and 55.0 mg of a tan powder was collected (105%; yield is assumed to be quantitative, as the solvation of the lithium cation of **1** may change over time). Crystals suitable for X-ray diffraction were grown from diethyl ether solutions with added THF cooled from room temperature to −35 °C. ^{1}H NMR (500 MHz, C_6D_6): δ/ppm: 80.08 (br s), 67.17 (br s), 58.22 (br s), 37.42 (br s), 25.82 (br s), 22.71 (br s), 14.40 (br s), 10.41 (br s), 9.19 (br s), 3.90 (br s), 1.49 (br s), −1.35 (br s), −9.37 (br s).

Computational Methods. Geometry optimzations were performed using the Gaussian 09 suite of software,[40] and population and electronic structure analyses were carried out using Gaussian 09 and the ORCA 2.8 suite.[41] Molecular geometries of complexes **2**−**7** were optimized using the X-ray crystal structure coordinates as input. Optimizations using both the BP86[42] pure DFT and M05-2X[43] hybrid functionals were attained, and for all complexes, the pure DFT functional (BP86) gave results that converged to lower energy structures that better matched the crystal structure geometries observed. Optimizations employed the TZVP[44] basis sets for the metal and first coordination sphere atoms, SVP[45] bases for all other atoms, and the W06[46] density fitting functional for density fitting approximations with BP86. A DFT population analysis was then carried out on the optimized geometries of complexes **2**−**6**, again

dx.doi.org/10.1021/ic402210j | *Inorg. Chem.* 2014, 53, 269−281

Scheme 2. Chemical Oxidations of Compound [(tpe)Fe(thf)]$^-$ (1)

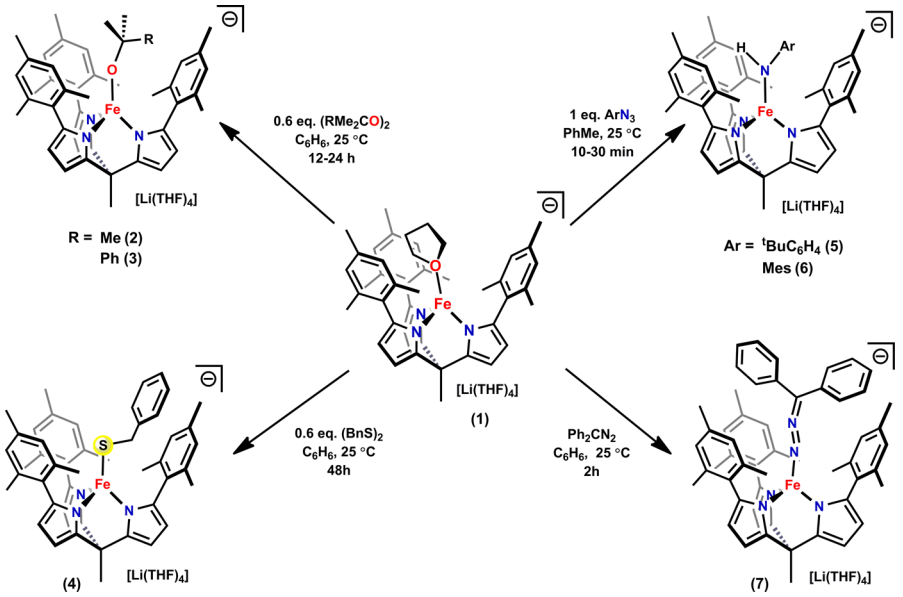

using the BP86 functional, using the TZV(P) and SV(P) basis sets. These analyses were deemed sufficient to describe the relatively straightforward electronic structures of the complexes.

The ORCA package was employed for correlation of optimized electronic structure to experimental data; Mössbauer parameters were calculated according to previously published procedures.[47] The B3LYP[48] functional has been found to give the best agreement with experimental data previously, and thus was used for Mössbauer parameter calculation here. The basis set used for iron was the core-prop basis, abbreviated CP(PPP)[49] and the bases for the remaining atoms were expanded to def2-TZVP[47a] for the coordination sphere and def2-SVP[43] for the remaining atoms. The def2-TZVP/J (Fe, N) and def2-SVP/J (C, H) auxiliary basis sets[47b] were employed to utilize the RIJCOSX[50] approximation for accelerating the calculation.

Given the uncertain spin ground state of complex 7, the geometry was optimized for complexes of S = 0, 1, 2, and 3. The lowest energy species was found to be the S = 2 complex, and this geometry was used for further calculations. To obtain more complete information about the J coupling found in the S = 2 complex 7, a broken symmetry calculation was performed as implemented in the ORCA suite. Specifically, a BS(5,1) system was investigated, denoting a system with five unpaired up spins and one unpaired down spin. Hybrid functionals have been shown to give better quantitative results, and thus the calculation was run using the B3LYP functional,[51] as well as the same bases used for the Mössbauer parameter calculations of **2**–**7** (vide supra). The broken symmetry solution was found to be approximately 1.0362 eV lower in energy than the high-spin solution. Indeed, the electronic structure described by the BS solution corresponds, qualitatively, very closely to the lowest-energy solution among those performed at all possible spin states, the S = 2 solution. The α- and β-orbital spatial overlap was estimated using the UHF Corresponding Orbitals method as implemented in ORCA.[52]

The coupling can be described by the use of a coupling term, J, as described by the Heisenberg–Dirac–van Vleck Hamiltonian (eq 1):

$$\hat{H} = -2J\hat{S}_A\hat{S}_B \quad (1)$$

This coupling term can be estimated using the Broken Symmetry method, wherein three methods of calculating J are useful for different coupling regimes (eqs 2–4).[51]

$$J^1_{AB} = \frac{^{LS}E - {}^{HS}E}{{S_{max}}^2} \quad (2)$$

$$J^2_{AB} = \frac{^{LS}E - {}^{HS}E}{S_{max}(S_{max}+1)} \quad (3)$$

$$J^3_{AB} = \frac{^{LS}E - {}^{HS}E}{{}^{HS}\langle S^2\rangle - {}^{LS}\langle S^2\rangle} \quad (4)$$

The method proposed by Bencini and Gatteschi,[53] found in eq 3, is most applicable to the strong-overlap limit, to which our results most closely apply, and thus has been used to estimate the coupling in this system. Molecular orbitals and spin density plots were generated from Gaussian cube files using Visual Molecular Dynamics 1.8.6[54] and rendered using POV-Ray v3.6[55] for Windows.

III. RESULTS

Synthesis. To assess whether metal-based redox activity is observable for (tpe)Fe complexes, we canvassed the reactivity of the anion [(tpe)Fe(THF)]$^-$ with a variety of one- and two-electron oxidants for which [(tpe)Fe(THF)]$^-$ is not a competent outer-sphere reductant, necessitating metal coordination for electron transfer to occur, if at all.[56] Reaction of brown-yellow [(tpe)Fe(THF)][Li(THF)$_4$] (**1**)[34] with 0.6 equiv of the single-electron oxidants di-*tert*-butyl peroxide, dicumyl peroxide, and dibenzyl disulfide in benzene over the course of 12–92 h results in formation of the ^{1}H NMR silent complexes of the type [(tpe)FeX][Li(THF)$_4$] (Scheme 2, X = O^{t}Bu (**2**), OCMe$_2$Ph (**3**), and SBn (**4**), respectively). The slow reaction times prohibit quantitative reaction, as both starting material and products are thermally sensitive and decompose at room temperature under a nitrogen atmosphere on the time scale of the reaction. Given the variability of THF solvation to the lithium countercation, accurate yields were determined by precipitating the product from diethyl ether by the addition of excess 12-crown-4. Displacement of THF from Li$^+$ with 12-crown-4 renders the complex insoluble in all relevant organic solvents to afford products with reliable [(tpe)FeX][Li(12-crown-4)$_2$] formulations. Yields for the peroxide reactions were found to be 86% (**2**) and 90% (**3**) by this method. Due to the slower reaction rate and competing thermal decomposition, a lower yield of 63% was found for compound **4**, but precipitation with 12-crown-4 was not necessary to obtain pure material. Crystals suitable for single-crystal X-ray

dx.doi.org/10.1021/ic402210j | Inorg. Chem. 2014, 53, 269–281

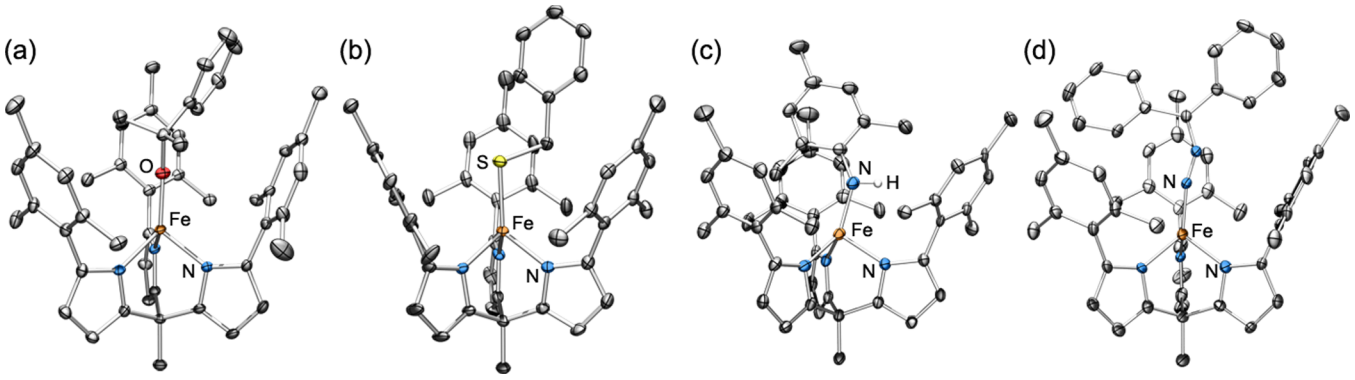

Figure 1. Solid state molecular structures of the anions in **3** (a), **4** (b), **6** (c), and **7** (d). Thermal ellipsoids are shown at 30% probability, and hydrogen atoms and solvated lithium countercations are omitted for clarity. Relevant bond distances (Å) and angles (deg) follow. For **3**: Fe−O, 1.778(3); Avg. Fe−N, 1.975(5); Fe−O−C_{cumyl}, 153.9(3). For **4**: Fe−S, 2.2381(11); Avg. Fe−N, 1.969(5); Fe−S−C_{benzyl}, 102.80(13). For **6**: Fe−N_{amido}, 1.890(5); Avg. Fe−N_{tpe}, 1.985(8); Fe−N−C_{aryl}, 141.9(4). For **7**: Fe−N_{diazo}, 1.781(9); Avg. Fe−N_{tpe}, 1.95(3); Fe−N−N_{diazo}, 160.3(8).

Table 1. Important Bond Metrics for Compounds 1 and 3−8

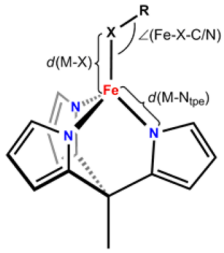

compound		average d(Fe−N_{tpe}) (Å)	Δd(Fe−N) from **1** (Å)	d(M−X) (Å)	∠(Fe−X−C/N) (deg)
[(tpe)Fe(THF)]$^-$	(**1**)[a,b]	2.022(5)		2.023(3)	
[(tpe)Fe($OCPhMe_2$)]$^-$	(**3**)	1.975(5)	−0.047	1.778(3)	153.9(3)
[(tpe)Fe(SBn)]$^-$	(**4**)	1.969(5)	−0.053	2.2381(11)	102.80(13)
[(tpe)Fe($NHC_6H_4{}^tBu$)]$^-$	(**5**)	1.9701(12)	−0.052	1.8836(7)	135.06(2)
[(tpe)Fe(NHMes)]$^-$	(**6**)	1.985(8)	−0.037	1.890(5)	141.9(4)
[(tpe)Fe(N_2CPh_2)]$^-$	(**7**)	1.955(29)	−0.067	1.781(9)	160.3(8)
[(tpe)Fe(PMe_3)]$^-$	(**8**)[b]	1.9986(3)	−0.023	2.3796(4)	
[(tpe)Fe(py)]$^-$	[b,c]	2.014(3)	−0.008	2.068(2)	

[a]From reference 34. [b]Compounds assigned as Fe^{2+} for comparison to those assigned as Fe^{3+}. Structural details can be found in the text. [c]From reference 29.

diffraction can be grown from concentrated solutions cooled to −35 °C (vide supra).

The addition of substituted aryl azides (4-^{t}Bu$C_6H_4N_3$, $MesN_3$) to **1** in benzene at room temperature produces dark, inky purple solutions over the course of minutes. Consumption of the starting material (**1**) was ascertained by monitoring the disappearance of the ^{1}H NMR resonances for **1** to the resultant ^{1}H NMR silent products. Additionally, the frequencies corresponding to azide N−N stretching frequencies in the IR spectrum disappear following reaction with **1**. Crystals suitable for single-crystal X-ray diffraction were grown from concentrated diethyl ether solutions with trace amounts of THF present at −35 °C. Solid state structure determination via X-ray diffraction confirmed the identity of the products as the iron−anilido complexes [(tpe)Fe(NHAr)][Li(THF)$_4$] [Scheme 2, Ar = 4-^{t}BuC_6H_4 (**5**), Mes (**6**)].

The addition of diphenyldiazomethane to complex **1** in thawing benzene over the course of 1 h results in a dark, inky green solution. Unlike the ^{1}H NMR silent species **2**−**6**, the reaction with diphenyldiazomethane exhibits a new paramagnetically shifted ^{1}H NMR spectrum distinct from **1** with 16 observable resonances. Furthermore, the resonant frequencies in the IR spectrum corresponding to the diazo stretching vibrations are no longer observable (free N_2CPh_2 $\upsilon_{C=N=N}$ = 2041 cm^{-1}, as determined by measurement of an authentic sample of N_2CPh_2). Crystals suitable for single-crystal X-ray diffraction were grown from a concentrated solution of the reaction product in *m*-xylene with trace amounts of THF, providing evidence for the formation of diazoalkane adduct [(tpe)Fe(N_2CPh_2)][Li(L)$_4$] (**7**, L = THF, Et_2O, Scheme 2).

Structural Elucidation. Given the paucity of NMR spectroscopic data for the reaction products **2**−**7**, reaction product identification was entirely dependent on molecular structure determination via X-ray diffraction analysis. The products of the above reactions, **2**−**7**, (Figure 1) all maintain iron coordinated to the trianionic tpe ligand in a $\kappa^1,\kappa^1,\kappa^1$-fashion, with a fourth apical ligand completing the coordination sphere. The apical ligand is unequivocally anionic for products **2**−**6**: alkoxides (**2** and **3**), benzylsulfide (**4**), or monoanionic anilido (**5** and **6**), suggesting in each oxidation reaction examined the oxidant has been chemically altered concomitant with oxidation of the iron center. Despite the oxidation, each complex remains anionic with a lithium countercation present,

dx.doi.org/10.1021/ic402210j | *Inorg. Chem.* 2014, 53, 269−281

Scheme 3. Reversible Electron Transfer Activated by Ligand Exchange of [(tpe)Fe] Complexes

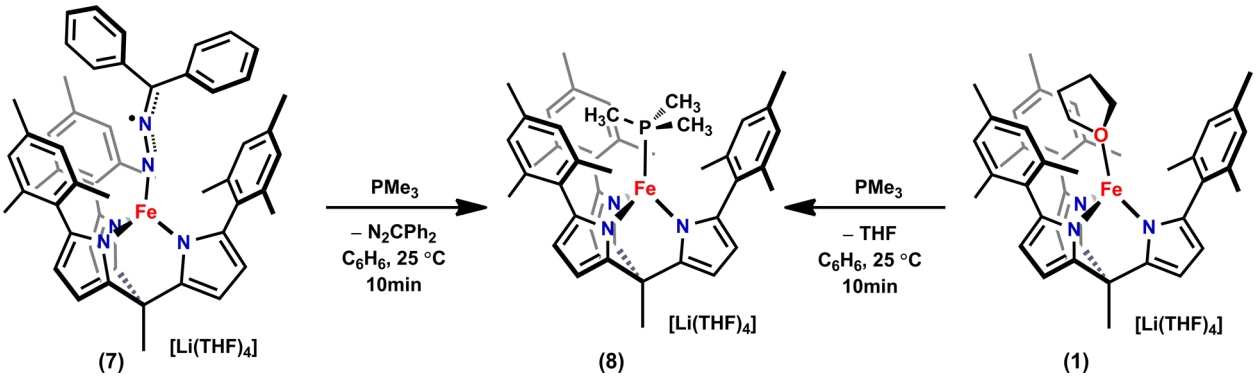

solvated by THF or diethyl ether as identified in each of the solid state molecular structures.

The positional disorder present in the structure of **2** does not permit rigorous determination of the bond metrics within the anion. The data acquired, however, was satisfactory to confirm the overall connectivity and identity of the anion. The crystal structures of **3** and **4** do not exhibit the same positional disorder for the tpe ligand, aided by the asymmetric nature of the alkoxide and thiolate ligands in the products. The steric differentiation provided by the ligands prevents positional variation in the tpe mesityl flanking units, permitting full refinement of the molecular structures. The solid state molecular structures of **3** and **4** are presented in Figure 1. The structures of the alkoxide products **2** and **3** confirm cleavage of the dialkyl peroxide O–O bond and formation of a new Fe–O bond in both cases, whereas the structure of benzyl sulfido **4** shows the analogous S–S bond breakage and Fe–S bond formation. The average Fe–N_{tpe} bond lengths are 1.975(5) Å for **3** and 1.969(5) Å for **4**, a shortening of ~0.05 Å compared to the bond lengths of the starting material, **1** (average d(Fe–N_{tpe}): 2.022(5) Å).[34] In addition, the oxygen atom of the cumyl alkoxide ligand in **3** is 0.245 Å closer to the iron (d(Fe–O): 1.778(3) Å) than the ethereal oxygen in the THF-adduct starting material, **1** (d(Fe–O): 2.023(3) Å), signifying increased π-donation between the alkoxide ligand and iron. The structural perturbations are summarized in Table 1.

The solid state molecular structures of the reaction products **5** and **6** resulting from azide oxidation are provided in the Supporting Information and Figure 1, respectively. In both structures, the organic azide oxidant has been converted into an anilido ligand, confirmed by location of the anilido hydrogen atom in the difference map during both crystal structure refinements. Following the structural determination of these reaction products, direct evidence of H-atom abstraction by reaction of **1** with organic azides was obtained using ^{1}H NMR spectroscopy. Using 1,3,5-trimethoxybenzene as an internal standard and 1,4-cyclohexadiene (CHD) as a H-atom donor (73 kcal/mol),[57] the disappearance of the ^{1}H resonances corresponding to a stoichiometric amount of CHD was observed in the reaction of **1** with both mesityl- and 4-^{t}BuC_6H_4-azide. This result suggests that in the absence of a weaker H-atom donor, THF or solvent is activated by a reaction intermediate (vide infra) to form products **5** and **6**.

The Fe–N_{tpe} distances average 1.970(1) Å in **5**, 1.985(8) Å in **6**, and are ca. 0.05 Å shorter than the 2.022(5) Å average Fe–N_{tpe} distances of compound **1**, mirroring the change observed for the one-electron oxidations observed in the structures for **3** and **4**. The Fe–$N_{anilido}$ bond lengths of 1.884(7) Å (**5**) and 1.890(5) Å (**6**) are shorter than the Fe–$N_{pyridine}$ distance of 2.068(2) Å found in the $[(tpe)Fe(py)]^-$ anion[29] and are most similar to known Fe^{3+} amido species.[58] The average Fe–N–C_{Ar} bond angle found for **5** is 135.06(2)° and the Fe–N–Ar bond angle for **6** is 141.9(4)°, values which are consistent with an anilido ligand featuring an sp^2 hybridized N bound to Fe.

Unlike the reactions of **1** with dialkyl peroxides, dialkyl disulfide, or aryl azides, the reaction of **1** with diphenyldiazoalkane results in the binding of the diazoalkane moiety without substantial structural modification of the diazoalkane. The solid state molecular structure of the anion for **7** (Figure 1d) features tpe-bound iron, with the diazoalkane ligand bound end-on completing the coordination sphere. Although the diazoalkane moiety is bound intact, the Fe—N_{tpe} bond lengths average 1.95(3) Å across the three structures found in the asymmetric unit, comparable to the average Fe—N_{tpe} found for compounds **2**–**6**, suggesting a redox transfer event has indeed taken place. The Fe—$N_{diazoalkane}$ distances average 1.781(9) Å, which is significantly shorter than known four-coordinate Fe—N_{amide} distances,[58,59] including those found for anilido complexes **5** and **6**. The average N—N and N—C bond lengths and Fe—N—N and N—N—C bond angles of the diazo moieties are 1.199(12) and 1.312(14) Å, and 160.3(8) and 148.5(11)°, respectively. These values are an unusual combination of bond lengths and angles for a diazoalkane complex, not, to our knowledge, found for any 3d transition metal species previously reported. Similar bond lengths are found for a bisphosphinoborate Cu complex (N—N = 1.163 and N—C 1.3188 Å), but the N—N—C bond angle of that complex is much closer to being linear (176.5°).[60] A similar N—N—C bond angle (150.4°) was found for a $[Cp(CO)_2Mn(N{=}NCO_2R)]$ complex, but the diazoalkane moiety resembles more closely the N—N triply bonded (1.165 Å), N—C singly bonded (1.351 Å) resonance structure, as well as featuring a much more linear M—N—N bond angle (176.9°).[61] The diazoalkane complex reported here features N—N—C and M—N—N bond angles between those expected for linear and trigonal planar bonding (sp and sp^2 hybridization), and the bond lengths are intermediate between N—N double and triple bonds and N—C double and single bonds, respectively. The only other reported iron diazoalkane adduct has shorter bond lengths along the M—N—N—C moiety and more linear bond angles, which is expected for a neutral donor type diazoalkane ligand.[62]

dx.doi.org/10.1021/ic402210j | Inorg. Chem. 2014, 53, 269–281

Table 2. Spectroscopic Parameters from Simulations of Low-Temperature X-band EPR data (4.3−6.0 K) and Measured by Zero-Field ^{57}Fe Mössbauer Spectroscopy (90 K) and SQUID Magnetometry for Compounds 2−7[a]

[(tpe)Fe(X)]$^-$		experimental (calculated)							
X		δ (mm/s)	$\lvert\Delta E_Q\rvert$ (mm/s)	g	D^b	E^b	E/D	ΔD^b	ΔE^b
THF	(**1**)	0.91	2.84						
O^{t}Bu	(**2**)	0.43 (0.42)	0.88 (−0.61)						
OCPhMe$_2$	(**3**)	0.38 (0.42)	1.00 (1.00)	1.99	0.380	0.063	0.17	0.06	0.013
SBn	(**4**)	0.36 (0.31)	1.01 (1.08)	1.99	0.747	0.123	0.16	0.001	0.025
NHC$_6$H$_4$^{t}Bu	(**5**)			1.99	0.663	0.113	0.17	0.15	0
NHMes	(**6**)	0.26 (0.40)	1.83 (1.16)						
N$_2$CPh$_2$	(**7**)	0.37 (0.38)	1.49 (−1.57)	2.01[c]	−3.27[c]	0.041[c]	0.01		
py		0.84	2.54						

[a]Experimental details can be found in the text. [b]Reported in units of cm^{-1}. [c]Measured by SQUID magnetometry.

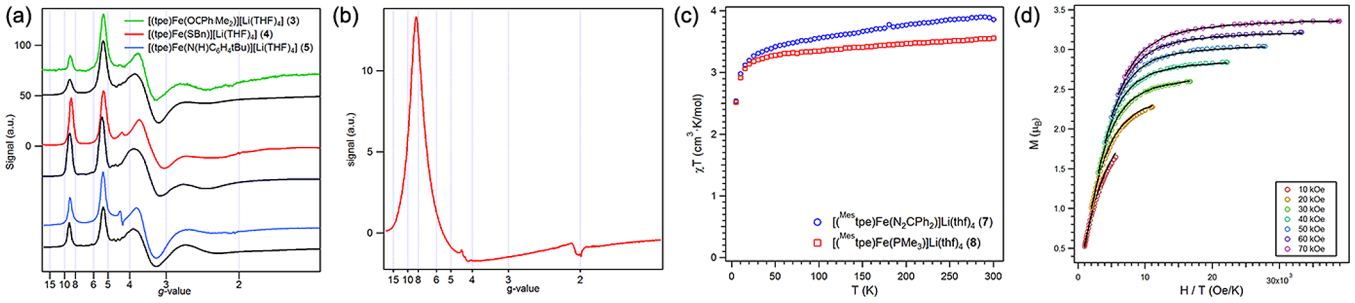

Figure 2. (a) Normalized 3.1 K X-band EPR spectra of compounds **3** (green), **4** (red), and **5** (blue) with simulated spectra appearing below the experimental data as solid black lines. Experimental details: microwave power = 0.6325 to 2.0 mW; modulation amplitude = 10 G; approximately 5 mmol concentration as a toluene glass. (b) Perpendicular mode X-band EPR spectrum of **7** taken at 4.3 K. (c) Variable-temperature magnetic susceptibility data for **7** (blue circles) and **8** (red squares) collected in an applied direct-current (DC) field of 10 kOe. (d) Plot of reduced magnetization for **7** between 1.8 and 10 K at selected fields.

To account for the tpe N—Fe bond contractions, which signify iron oxidation in **7**, the diazoalkane moiety must be concomitantly reduced by one electron. Chemical transformation of the diazoalkane (i.e., H-atom abstraction to the N_2CPh_2 unit) was ruled out by examining the ability of **7** to undergo diazoalkane release. Treatment of complex **7** with excess PMe_3 in benzene resulted in an instantaneous change from dark, inky green to a pale brown-yellow color similar to the color of the THF adduct **1**. Tertiary phosphine ligand exchange is confirmed by ^{1}H NMR spectroscopy, as the paramagnetically shifted resonances of **7** disappear, giving way to a new paramagnetically shifted ^{1}H spectrum for the ferrous complex [(tpe)Fe(PMe_3)][Li(THF)$_4$] (**8**, Scheme 3). An authentic sample of **8** can be obtained by simple addition of excess PMe_3 to starting material **1**, which features an identical ^{1}H NMR to the spectrum obtained from the diazoalkane displacement reaction above. If product **7** had undergone a chemical transformation following one-electron reduction (i.e., H-atom abstraction analogous to the azide oxidations), the modified diazoalkane ligand should not readily exchange with the neutral donor PMe_3.

Although the oxidation of the iron centers is demanded by charge balance in complexes **2**−**7** following the addition of the fourth anionic ligand to the iron coordination sphere, we sought to rigorously establish that the tpe ligand itself did not manifest changes signifying its participation in the observed redox event. If the pyrrolide subunits contribute to the observed redox event, we would anticipate substantial changes in the pyrrolic C−C and C−N bond distances. Similar bond length alterations in similar redox-active ligand platforms are hallmark redox signifiers. Changes in pyrrole C−C and C−N distances after oxidation were all smaller than 3σ and thus considered insignificant. This observation supports that oxidation is primarily iron-centered and is not borne by the pyrrolides of the ligand. By way of comparison, the known redox-active ligand system α-iminopyridine exhibits successive C−C and C−N bond elongations of 0.06 Å per one-electron reduction of the ligand.[18c] Aromatic C−C bond elongation of 0.027 Å is observed in the oxidation from phenylenediamine to the di(isobutyl)iminosemiquinone ligands.[63] All of these ligand alterations are readily observed and statistically significant.

Zero-Field ^{57}Fe Mössbauer Spectroscopy. Complexes **2**−**4** exhibit single quadrupole doublets in the ^{57}Fe Mössbauer spectra at 90 K, with isomer shifts (δ) of 0.43, 0.38, and 0.36 mm/s, and quadrupole splittings ($\lvert\Delta E_Q\rvert$) of 0.88, 1.00, and 1.01 mm/s, respectively. Aryl anilido product **6** has an isomer shift of 0.26 mm/s and a quadrupole splitting of 1.83 mm/s. The isomer shift value is the lowest of the Fe^{3+} complexes we have isolated, but still well within the range of typical values for four-coordinate Fe^{3+} ions.[64] Finally, diphenyldiazomethane adduct **7** gives Mössbauer parameters remarkably similar to complexes **2**−**4**, with an isomer shift of = 0.37 mm/s and quadrupole splitting of $\lvert\Delta E_Q\rvert$ = 1.49 mm/s. Mössbauer data are summarized in Table 2.

X-band EPR Spectroscopy. X-band EPR spectra at 3.1 K of toluene glasses complexes **3**, **4** and **5**, shown in Figure 2a, exhibit features at g_{eff} = 8.72, 5.17, 3.41, and 2.31 (complex **3**); g_{eff} = 8.66, 5.27, 3.33, and 2.27 (complex **4**); g_{eff} = 8.69, 5.18, 3.41, and 2.30 (complex **5**). The spectra for alkoxide **3** and benzyl sulfido **4** can be simulated as S = 5/2 spin systems (Figure 2a, Table 2) with isotropic g values of 1.988 and 1.995, respectively. The complexes show appreciable zero-field

dx.doi.org/10.1021/ic402210j | Inorg. Chem. 2014, 53, 269−281

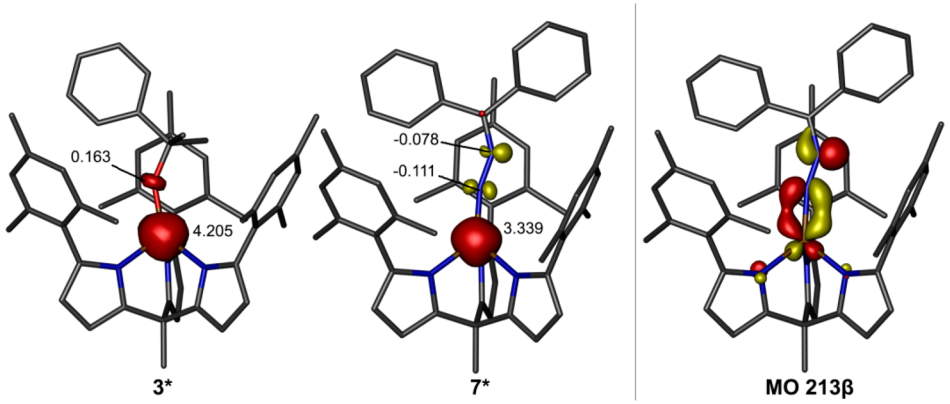

Figure 3. (Left) spin polarization density plots (α and β, shown at isovalue 0.01) from single-point energy calculations of sextet **3*** and quintet **7***. Bases, functionals and methods are described in the Experimental Section details. Net α-spin density is shown in red and net β-spin density in yellow. Atoms are labeled with their Mulliken spin population for iron and nitrogens possessing appreciable spin density. Hydrogen atoms are omitted for clarity. No localized net β-spin density is observed for the high-spin **3***, whereas significant spatial separation between net α- and β-spins exists for structure **7***, leading to antiferromagnetic coupling between the Fe and ligand N atoms. (Right) occupied metal-L(π*) molecular orbital responsible for the β-spin polarization density observed (isovalue 0.08).

splitting (ZFS), with axial ZFS (D) of 0.379 cm^{-1} and 0.748 cm^{-1}, respectively, and both show intermediate amounts of rhombicity, with values of E/D of 0.168 for **3** and 0.164 for **4**. The line breadth can be accounted for by including significant amounts of D and E strain (ΔD = 0.061 and 0.0012 cm^{-1}, ΔE = 0.013 and 0.025 cm^{-1}, respectively) in the simulations. The spectrum of aryl amide **5** bears a striking similarity to alkoxides **2** and **3** and alkylsulfide complex **4** and can also be simulated as an S = 5/2 spin high-spin Fe^{3+} system very similarly to complexes **3** and **4**. The simulation employs an isotropic g = 1.990 and an anisotropic zero-field splitting with D = 0.664 cm^{-1} and E = 0.115 cm^{-1}, resulting in an E/D of 0.173. In this case, only D strain (ΔD = 0.154 cm^{-1}) is needed to simulate the line broadening adequately. In all three cases, the features at roughly g_{eff} = 8.7 and 2.3 are transitions of components of the $m_s = \pm 1/2$ states, and the 5.2 and 3.4 g_{eff} features are $m_s = \pm 3/2$ state transitions. It is likely the $m_s = \pm 5/2$ states are of high enough energy that they are unpopulated and unobserved.

The X-band EPR spectrum of **7** at 4.3 K is shown in Figure 2b and does not resemble complexes **2**−**5**, instead displaying one major feature at g_{eff} = 8.34. This resembles S = 2 spin systems reported in the literature.[65] ^{1}H NMR spectroscopy corroborates this assignment, as a spectrum with distinct resonances is observed for complex **7**, whereas complexes **2**−**4**, simulated as S = 5/2 systems, are ^{1}H NMR silent. We hypothesized that the EPR spectrum observed for complex **7** represents an observable non-Kramers doublet of an integer spin system, and we turned to magnetic measurements to interrogate this possibility.

Magnetism. Variable temperature (VT) direct-current (DC) susceptibility data were collected from 5 to 300 K (Figure 2c) in a field of 10 000 Oe. For complex **8**, the average value of $\chi_M T$ in the temperature range of 50−300 K (the region for which we deem the Curie Law is applicable) was 3.43 cm^3 K/mol. The data for diphenyldiazomethane complex **7** do not differ greatly from the data for **8**, with an average $\chi_M T$ between 50 and 300 K of 3.44 cm^3 K/mol. The values obtained for complex **8** are close to the value expected for a spin-only S = 2 system (3.00 cm^3 K/mol), as expected for a high-spin Fe^{2+} complex. Complex **7** exhibits strikingly similar values, suggesting that the overall spin ground state of **7** is S = 2.

A plot of reduced magnetization for **7** was obtained from VT data collected between 1.8 and 10 K at seven fields between 10 and 70 kOe (Figure 2d). The resulting plot shows non-superimposable isofield curves, indicative of zero-field splitting present in complex **7**. Using the Hamiltonian in eq 5, the reduced magnetization data was fit using the program ANISOFIT,[37] and reasonable values of g could only be obtained when fitting the system as an S = 2 ground state. The fitting parameters obtained are included in Table 2.

$$\hat{H} = \mu_B g H \cdot \hat{S} + D\hat{S}_z^{\,2} + E(\hat{S}_x - \hat{S}_y)^2 \qquad (5)$$

If the diazoalkane were to bind as a neutral donor ligand, an S = 5/2 ground state would be expected for the Fe^{3+} spin system, as determined by Mössbauer spectroscopy (vide supra). To satisfy the S = 2 ground state suggested by the magnetic data, we propose a system that features antiferromagnetic coupling of a diazoalkanyl radical (S = 1/2) to an S = 5/2 Fe^{3+}.

Density Functional Theory. DFT calculations were employed to establish the nature of the electronic spin ground states of complexes **2**−**7**. The crystal structure coordinates were optimized in a variety of spin states, and the lowest energy spin state was confirmed to be S = 5/2 for **2***−**6*** and S = 2 for **7*** (an asterisk indicates the geometry optimized coordinates of the complex). The Mössbauer parameters of the lowest energy optimized structures were calculated to correlate the resultant optimized structures with experimental data and matched remarkably well (Table 2).[47,49,66]

Broken symmetry calculations were employed to investigate the strength of the coupling between the iron center and the diazoalkanyl radical for structure **7***. The α- and β-orbital spatial overlap was estimated to be 74.9%, suggesting significant localized orbital character. The antiferromagnetic exchange coupling parameter ($J^{(2)}$) was found to be −696 cm^{-1}. A spin density plot of the optimized, quintet diazoalkane adduct clearly shows this antiferromagnetic coupling, as the net α-spin is localized mainly on the iron atom and the net β-spin populates the π-bonding molecular orbital of the N−N fragment of the diazoalkane. This plot is presented alongside a spin density plot of the cumyl oxido structure for comparison in Figure 3. These DFT calculations also describe an overall S = 2 system featuring an S = 5/2 iron center antiferromagnetically

dx.doi.org/10.1021/ic402210j | Inorg. Chem. 2014, 53, 269−281

Scheme 4. Proposed Mechanism of Inner-Sphere Oxidation of 1 by Dialkyl Peroxides and Dialkyl Disulfides

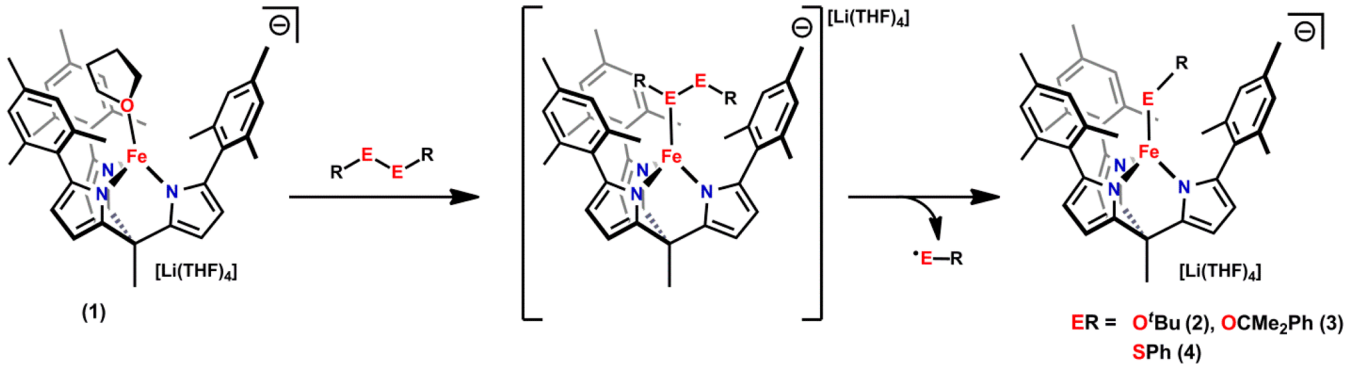

Scheme 5. Proposed mechanism of inner-sphere oxidation of 1 by organic azides

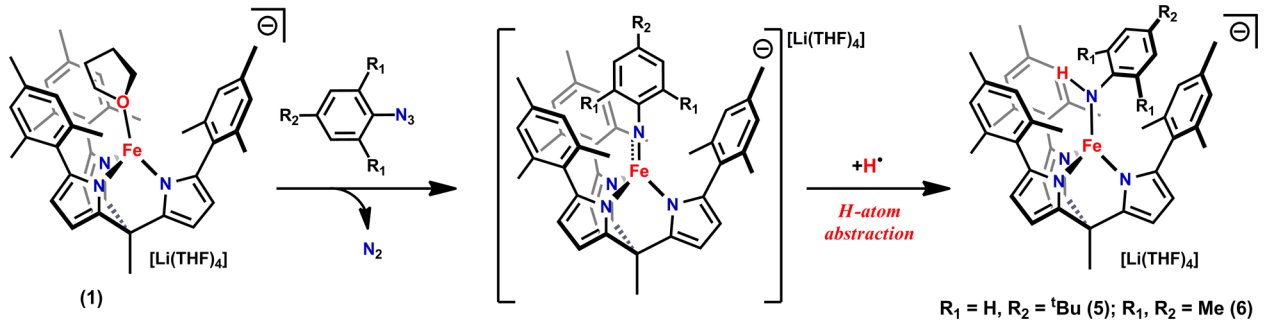

coupled to an $S = 1/2$ ligand-based radical, as deduced from experimental data.

IV. DISCUSSION

The foregoing structural and spectroscopic analysis indicate the [(tpe)Fe(THF)]$^-$ synthon can undergo oxidation with concomitant reduction of dialkyl peroxide, dialkyl disulfide, aryl azides, and even diazoalkane substrates. The majority of the oxidation products, with the exception of **7**, are ^{1}H NMR silent, and structural determination by X-ray crystallographic analysis provides a starting point to understand the reaction products. To balance charges after addition of alkoxide (**2** and **3**) and benzyl sulfido (**4**) ligands, products **2**−**4** should feature a formally Fe^{3+} oxidation state following reaction. The redox potential of **1** is insufficient to reduce the dialkyl peroxides via an outer-sphere mechanism,[56] suggesting the dialkyl peroxide, and by extension, dibenzyl disulfide reagents must coordinate the metal center prior to electron transfer to induce O−O or S−S bond cleavage (Scheme 4). A similar reaction pathway has been invoked in the (nacnac)Cu mediated reduction of di-*tert*-butyl peroxide.[67]

Reaction with organic azides results in complexes wherein, after the identification of the apical ligands in **5** and **6** as monoanionic anilido moieties, charge balance also suggests an Fe^{3+} formulation. Conversion of organic azides to amide ligands typically occurs via azide breakdown following coordination to the transition metal center to produce either imido radical[47a] or closed-shell imido products.[68] The former results from single electron transfer to the azide, whereas the latter from full two-electron oxidation of the metal center. Both intermediates have been shown to be competent for H-atom abstraction reactions and are viable intermediates on the pathway of **1** to anilido products **5** and **6** (Scheme 5). Given the observed propensity of pyrrolido ligand-bound iron(II) complexes to undergo single electron transfer events (vide supra), we propose the imido radical intermediate might be operative in this example.

Charge balance is not reliable as an indicator of iron oxidation state for the structure obtained for product **7**, as the diazoalkane ligand could be bound as a neutral ligand or a doubly reduced ligand to adopt an imido-like metal−ligand multiple bond.[69] The bond metrics obtained can, however, be compared to those of structures of **2**−**6**. Product **7** exhibits a shortening of the Fe−$N_{pyrrolido}$ distances similar in magnitude to that found for **2**−**6**. Additionally, the Fe−N_{diazo} bond distance is shorter than the Fe−$N_{anilido}$ bond length found for **5** and **6**, indicating a further interaction than would be expected between a neutral donor diazoalkane ligand and iron.[62] Further spectroscopic examination served to elucidate this interaction.

Zero-field, ^{57}Fe Mössbauer spectroscopy allows us to assess specifically the oxidation state at iron. The complexes remain four-coordinate following each reaction, thus the isomer shifts provide a straightforward indicator of iron oxidation state; the marked isomer shift decreases of 0.48 to 0.65 mm/s from the Fe^{2+} starting material, **1**, (δ = 0.91mm/s) are strongly indicative of reduced electron density at the Fe atom, suggesting one-electron oxidations have occurred. Comparison of the quadrupole splitting values of complexes **2**−**4** to the known Fe^{2+} species ($|\Delta E_Q|$ = 2.84) shows decreases ranging from 1.81 to 1.96 mm/s. In idealized C_{3v} symmetry, oxidation of a d^6 high-spin Fe^{2+} complex to a d^5 high-spin Fe^{3+} removes the single β electron responsible for the asymmetric population of the low-lying e $(x^2 - y^2, xy)^3$ set, resulting in a higher symmetry electron distribution at iron after oxidation, and thus a lower quadrupole splitting. The Fe^{3+} assignment is also affirmed by Mössbauer for a representative product of reaction of **1** with organic azide (**6**) as well. The EPR data collected corroborates these assignments, as EPR spectra of this shape have been observed previously for four-coordinate high-spin Fe^{3+}

dx.doi.org/10.1021/ic402210j | Inorg. Chem. 2014, 53, 269−281

complexes, including Fe^{III}-catecholate models of DOPA-containing mussel glue precursor proteins,[70] nonheme Fe^{III}–OOR superoxide reductase model complexes,[71] and synthetic Fe^{III} hydroxide complexes.[72] The magnitude of the zero-field splitting is also similar to these biological and synthetic high-spin Fe^{3+} systems reported in the literature.

The Mössbauer parameters acquired for **7**, along with the crystallographic data, allow us to unambiguously assign the oxidation state of iron in compound **7** as Fe^{3+}. Given the overall spin of $S = 2$ suggested by EPR and SQUID magnetometry together with the formulation of Fe^{3+}, we are also able to assign the oxidation state of the diazoalkane ligand. To achieve an overall spin of $S = 2$, the diazoalkane ligand must be a radical anion with $S = 1/2$, antiferromagnetically coupled to the $S = 5/2$ Fe^{3+}. This explanation also provides a rationale for the unusually short $Fe-N_{diazo}$ bond distance.

By way of comparison to tpe iron complexes, previously reported examples of redox-active ligand systems feature metal and ligand molecular orbitals fully conjugated with one another and comprise a single molecular redox entity. This is typically observed for binding of the redox-active chelates onto the metal in a geometry that maximizes π-orbital overlap with the metal-based orbitals of appropriate symmetry, generating an orbital pathway that brings both redox reservoirs into conjugation.[3,6−18] In these literature examples, oxidations proceed from the highest to lowest energy molecular orbitals, regardless of oxidation mechanism, permitting the molecular entity to traverse several consecutive redox events. With the $[(tpe)M]^-$ species, the weakly σ-donating pyrrolides[73] enforce a tetrahedral-like geometry at the bound metal center. This geometric restriction, in concert with the weak-field ligand, conspires to engender open-shell configurations for the resulting coordination complexes, diminishing any π-orbital overlap between the pyrrolides and the metal center, thereby mitigating any available orbital overlap to connect the two redox reservoirs. As a result, the two disparate redox reservoirs are accessible by the different oxidation mechanisms.

The reversible electron transfer to and from the diphenyldiazomethane provides further insight into the ligand–metal redox communication process. The diphenyldiazomethane ligand features a low lying π^*-system with the proper orientation and energetic overlap to allow facile inner-sphere electron transfer from the Fe-based orbitals of π-symmetry. The resulting radical anion is delocalized within the diazoalkane N–N π-system, stabilized by steric protection provided by the (tpe) mesityl units and the CPh_2 terminus of the diazoalkane itself. In this case, the Fe–N bond is quite strong, being significantly shorter than the Fe–N bonds found in the anilido complexes **5** and **6** and even the putative imido radical observed on the related dipyrrin ligand platform.[47a] Provided an orbital coupling pathway for electron transfer between metal and ligand, such as present in the diazoalkane adduct, redox communication becomes kinetically facile. In the absence of this orbital conjugation or a large enough thermodynamic driving force for outer-sphere transfer, coordination complexes exhibiting both type A and B behavior are observed, featuring disparate redox reservoirs accessible by different oxidation mechanisms.

V. CONCLUSIONS

We have shown that tris(pyrrolido)ethane complexes of Fe^{2+} are capable of inner-sphere oxidation, whether one- or two-electron oxidants are employed. In the case of two-electron oxidation, the resultant two-electron oxidized species is unstable and undergoes a H-atom abstraction, resulting in a net single-electron oxidized product.

X-ray crystallography allows for direct comparison of the Fe^{2+} starting materials with the products reported and suggests oxidation at iron upon reaction. An appreciable change in ^{57}Fe Mössbauer isomer shifts was observed for complexes **2**–**7**, which is a particularly good indicator of iron-specific oxidation. Low-temperature X-band EPR spectroscopy confirms the oxidation states suggested by the Mössbauer data and solidifies the $S = 5/2$ spin state of complexes **2**–**6** and reveals an $S = 2$ spin state of diazoalkane complex **7**. Taken together, these data unambiguously establish the oxidation state of iron to be 3+, in spite of the known redox liability of the tpe ligand. Removal of the diazoalkane ligand by reaction with a stronger donor demonstrates the feasibility of reversing this oxidation.

Outer- and inner-sphere electron transfers from [(tpe)Fe-(THF)] are localized oxidations accessing different redox reservoirs. Oxidation is specific to the redox reservoir accessed, with no electron transfer between reservoirs. Outer-sphere electron transfer (via chemical or electrochemical means) is dominated by the ligand pyrrolide subunits, whereas inner-sphere chemical oxidation is mediated by the transition metal.

■ ASSOCIATED CONTENT

Supporting Information

Crystallographic data (CIF file) for complexes **2**–**8**. This material is available free of charge via the Internet at http://pubs.acs.org.

■ AUTHOR INFORMATION

Corresponding Author

*T. A. Betley. E-mail: betley@chemistry.harvard.edu.

Notes

The authors declare no competing financial interest.

■ ACKNOWLEDGMENTS

The authors thank Harvard University and the NSF (CHE-095585) for funding. T.A.B. is grateful for a George W. Merck Fellowship. G.T.S. thanks the NSF GRFP for funding. We thank Dr. Yu-Sheng Chen at ChemMatCARS, Advanced Photon Source, for his assistance with single-crystal data. ChemMatCARS Sector 15 is principally supported by the National Science Foundation/Department of Energy under grant number NSF/CHE-0822838. Use of the Advanced Photon Source was supported by the U.S. Department of Energy, Office of Science, Office of Basic Energy Sciences, under Contract No. DE-AC02-06CH11357. We thank Dr. Shao-Liang Zheng for assistance with crystallography.

■ REFERENCES

(1) (a) Taube, H.; Myers, H.; Rich, R. L. *J. Am. Chem. Soc.* **1953**, *75*, 4118–4119. (b) Taube, H.; Gould, E. S. *Acc. Chem. Res.* **1969**, *2*, 321–329. (c) Taube, H. *Science* **1984**, *226*, 1028–1036.

(2) (a) Vaska, L.; DiLuzio, J. W. *J. Am. Chem. Soc.* **1962**, *84*, 679–680. (b) Johnson, C. E.; Eisenberg, R. *J. Am. Chem. Soc.* **1985**, *107*, 3148–3160.

(3) Chaudhuri, P.; Verani, C. N.; Bill, E.; Bothe, E.; Weyhermüller, T.; Wieghardt, K. *J. Am. Chem. Soc.* **2001**, *123*, 2213–2223.

(4) Jørgensen, C. K. *Coord. Chem. Rev.* **1966**, *1*, 164–178.

(5) A thoroughly investigated case study of these types of ligand-based orbitals is presented for $[Ni(MNT)_2]$ complexes: (a) Szilagyi, R. K.; Lim, B. S.; Glaser, T.; Holm, R. H.; Hedman, B.; Hodgson, K. O.;

Solomon, E. I. *J. Am. Chem. Soc.* **2003**, *125*, 9158−9169. (b) Sarangi, R.; DeBeer George, S.; Rudd, D. J.; Szilagyi, R. K.; Ribas, X.; Rovira, C.; Almeida, M.; Hodgson, K. O.; Hedman, B.; Solomon, E. I. *J. Am. Chem. Soc.* **2007**, *129*, 2316−2326.

(6) (a) Schrauzer, G. N.; Mayweg, V. *J. Am. Chem. Soc.* **1962**, *84*, 3221. (b) Gray, H. B.; Williams, R.; Bernal, I.; Billig, E. *J. Am. Chem. Soc.* **1962**, *84*, 3596−3597. (c) Gray, H. B.; Billig, E. *J. Am. Chem. Soc.* **1963**, *85*, 2019−2020. (d) Davison, A.; Edelstein, N.; Holm, R. H.; Maki, A. H. *Inorg. Chem.* **1963**, *2*, 1227−1232. (e) Eisenberg, R.; Gray, H. B. *Inorg. Chem.* **2011**, *50*, 9741−9751.

(7) (a) Haga, M.; Dodsworth, E. S.; Lever, A. B. P. *Inorg. Chem.* **1986**, *25*, 447−453. (b) Masui, H.; Lever, A. B. P.; Auburn, P. R. *Inorg. Chem.* **1991**, *30*, 2402−2410.

(8) (a) Hockertz, J.; Steenken, S.; Wieghardt, K.; Hildebrandt, P. *J. Am. Chem. Soc.* **1993**, *115*, 11222−11230. (b) Chaudhuri, P.; Hess, M.; Muller, J.; Hildenbrand, K.; Bill, E.; Weyhermüller, T.; Wieghardt, K. *J. Am. Chem. Soc.* **1999**, *121*, 9599−9610.

(9) (a) Herebian, D.; Bothe, E.; Bill, E.; Weyhermüller, T.; Wieghardt, K. *J. Am. Chem. Soc.* **2001**, *123*, 10012−10023. (b) Blackmore, K. J.; Ziller, J. W.; Heyduk, A. F. *Inorg. Chem.* **2005**, *44*, 5559−5561. (c) Haneline, M. R.; Heyduk, A. F. *J. Am. Chem. Soc.* **2006**, *128*, 8410−8411. (d) Blackmore, K. J.; Lal, N.; Ziller, J. W.; Heyduk, A. F. *J. Am. Chem. Soc.* **2008**, *130*, 2728−2729. (e) Wright, D. D.; Brown, S. N. *Inorg. Chem.* **2013**, *52*, 7831−7833.

(10) (a) Lionetti, D.; Medvecz, A. J.; Ugrinova, V.; Quiroz-Guzman, M.; Noll, B. C.; Brown, S. N. *Inorg. Chem.* **2010**, *49*, 4687−4697. (b) Kopec, J. A.; Shekar, S.; Brown, S. N. *Inorg. Chem.* **2012**, *51*, 1239−1250.

(11) (a) Heyduk, A. F.; Zarkesh, R. A.; Nguyen, A. I. *Inorg. Chem.* **2011**, *50*, 9849−9863. (b) Munhá, R. F.; Zarkesh, R. A.; Heyduk, A. F. *Inorg. Chem.* **2013**, *52*, 11244−11255.

(12) (a) Szigethy, G.; Heyduk, A. F. *Inorg. Chem.* **2011**, *50*, 125−135. (b) Clark, K. M.; Bendix, J.; Heyduk, A. F.; Ziller, J. W. *Inorg. Chem.* **2012**, *51*, 7457−7459.

(13) (a) Bouwkamp, M. W.; Bowman, A. C.; Lobkovsky, E.; Chirik, P. J. *J. Am. Chem. Soc.* **2006**, *128*, 13340−13341. (b) Bart, S. C.; Chlopek, K.; Bill, E.; Bouwkamp, M. W.; Lobkovsky, E.; Neese, F.; Wieghardt, K. *J. Am. Chem. Soc.* **2006**, *128*, 13901−13912. (c) Bart, S. C.; Lobkovsky, E.; Bill, E.; Wieghardt, K.; Chirik, P. J. *Inorg. Chem.* **2007**, *46*, 7055−7063. (d) Myers, T. W.; Berben, L. A. *J. Am. Chem. Soc.* **2013**, *135*, 9988−9990. (e) Myers, T. W.; Berben, L. A. *Organometallics* **2013**, *32* (22), 6647−6649.

(14) (a) Lu, C. C.; Bill, E.; Weyhermüller, T.; Bothe, E.; Wieghardt, K. *J. Am. Chem. Soc.* **2008**, *130*, 3181−3197. (b) Muresan, N.; Lu, C. C.; Ghosh, M.; Peters, J. C.; Abe, M.; Henling, L. M.; Weyhermüller, T.; Bill, E.; Wieghardt, K. *Inorg. Chem.* **2008**, *47*, 4579−4590. (c) Lu, C. C.; Weyhermüller, T.; Bill, E.; Wieghardt, K. *Inorg. Chem.* **2009**, *48*, 6055−6064. (d) Myers, T. W.; Kazem, N.; Stoll, S.; Britt, R. D.; Shanmugam, M.; Berben, L. A. *J. Am. Chem. Soc.* **2011**, *133*, 8662−8672. (e) Myers, T. W.; Berben, L. A. *J. Am. Chem. Soc.* **2011**, *133*, 11865−11867. (f) Myers, T. W.; Berben, L. A. *Inorg. Chem.* **2012**, *51*, 1480−1488. (g) Myers, T. W.; Holmes, A. L.; Berben, L. A. *Inorg. Chem.* **2012**, *51*, 8897−8903. (h) Cates, C. D.; Myers, T. W.; Berben, L. A. *Inorg. Chem.* **2012**, *51*, 11891−11897.

(15) (a) Flores, J. A.; Andino, J. G.; Tsvetkov, N. P.; Pink, M.; Wolfe, R. J.; Head, A. R.; Lichtenberger, D. L.; Massa, J.; Caulton, K. G. *Inorg. Chem.* **2011**, *50*, 8121−8131. (b) Tsvetkov, N. P.; Chen, C.-H.; Andino, J. G.; Lord, R. L.; Pink, M.; Buell, R. W.; Caulton, K. G. *Inorg. Chem.* **2013**, *52*, 9511−9521.

(16) (a) Frazier, B. A.; Wolczanski, P. T.; Lobkovsky, E. B.; Cundari, T. R. *J. Am. Chem. Soc.* **2009**, *131*, 3428−3429. (b) Hulley, E. B.; Wolczanski, P. T.; Lobkovsky, E. B. *J. Am. Chem. Soc.* **2011**, *133*, 18058−18061. (c) Frazier, B. A.; Bartholomew, E. R.; Wolczanski, P. T.; DeBeer, S.; Santiago-Berrios, M.; Abruna, H. D.; Lobkovsky, E. B.; Bart, S. C.; Mossin, S.; Meyer, K.; Cundari, T. R. *Inorg. Chem.* **2011**, *50*, 12414−12436. (d) Frazier, B. A.; Wolczanski, P. T.; Keresztes, I.; DeBeer, S.; Lobkovsky, E. B.; Pierpont, A. W.; Cundari, T. R. *Inorg. Chem.* **2012**, *51*, 8177−8186. (e) Frazier, B. A.; Williams, V. A.; Wolczanski, P. T.; Bart, S. C.; Meyer, K.; Cundari, T. R.; Lobkovsky, E. B. *Inorg. Chem.* **2013**, *52*, 3295−3312.

(17) (a) Zarkesh, R. A; Ziller, J. W.; Heyduk, A. F. *Angew. Chem., Int. Ed.* **2008**, *47*, 4715−4718. (b) Zarkesh, R. A.; Heyduk, A. F. *Organometallics* **2011**, *30*, 4890−4898.

(18) (a) Small, B. L.; Brookhart, M. *J. Am. Chem. Soc.* **1998**, *120*, 7143−7144. (b) Scarborough, C. C.; Sproules, S.; Weyhermüller, T.; DeBeer, S.; Wieghardt, K. *Inorg. Chem.* **2011**, *50*, 12446−12462. (c) Lu, C. C.; DeBeer George, S.; Weyhermüller, T.; Bill, E.; Bothe, E.; Wieghardt, K. *Angew. Chem., Int. Ed.* **2008**, *47*, 6384−6387. (d) Britovsek, G. J. P.; Gibson, V. C.; McTavish, S. J.; Solan, G. A.; White, A. J. P.; Williams, D. J.; Kimberley, B. S.; Maddox, P. J. *Chem. Commun.* **1998**, 849−850. (e) Smith, A. L.; Hardcastle, K. I.; Soper, J. D. *J. Am. Chem. Soc.* **2010**, *132*, 14358−14360. (f) Tondreau, A. M.; Atienza, C. C. H.; Weller, K. J.; Nye, S. A.; Lewis, K. M.; Delis, J. G. P.; Chirik, P. J. *Science* **2012**, *335*, 567−570. (g) Shaffer, D. W.; Szigethy, G.; Ziller, J. W.; Heyduk, A. F. *Inorg. Chem.* **2013**, *52*, 2110−2118.

(19) (a) Schulz, C. E.; Devaney, P. W.; Winkler, H.; Debrunner, P. G.; Doan, N.; Chiang, R.; Rutter, R.; Hager, L. P. *FEBS Lett.* **1979**, *103*, 102−105. (b) Groves, J. T.; Haushalter, R. C.; Nakamura, M.; Nemo, T. E.; Evans, B. J. *J. Am. Chem. Soc.* **1981**, *103*, 2884−2886. (c) Penner-Hahn, J. E.; Smith Eble, K.; McMurry, T. J.; Renner, M.; Balch, A. L.; Groves, J. T.; Dawson, J. H.; Hodgson, K. O. *J. Am. Chem. Soc.* **1986**, *108*, 7819−7825.

(20) Watanabe, Y. In *The Porphyrin Handbook*; Kadish, K. M., Smith, K. M., Guilard, R., Eds.; Academic Press: NewYork, 2000; Vol. *4*, pp 97−118.

(21) (a) Kim, S. H.; Perera, R.; Hager, L. P.; Dawson, J. H.; Hoffman, B. M. *J. Am. Chem. Soc.* **2006**, *128*, 5598−5599. (b) Hocking, R. K.; Wasinger, E. C.; Yan, Y.-L.; Degroot, F. M. F.; Walker, F. A.; Hodgson, K. O.; Hedman, B.; Solomon, E. I. *J. Am. Chem. Soc.* **2007**, *129*, 113−125.

(22) Rittle, J.; Green, M. T. *Science* **2010**, *330*, 933−937.

(23) Meier-Callahan, A. E.; Di Bilio, A. J.; Simkhovich, L.; Mahammed, A.; Goldberg, I.; Gray, H. B.; Gross, Z. *Inorg. Chem.* **2001**, *40*, 6788−6793.

(24) (a) Floriani, C.; Floriani-Moro, R. In *The Porphyrin Handbook*; Academic Press: San Diego, CA, 2003; Vol. *3*, pp 405−420. (b) Jubb, J.; Floriani, C.; Chiesi-Villa, A.; Rizzoli, C. *J. Am. Chem. Soc.* **1992**, *114*, 6571−6573. (c) Piarulli, U.; Solari, E.; Floriani, C.; Chiesi-Villa, A.; Rizzoli, C. *J. Am. Chem. Soc.* **1996**, *118*, 3634−3642. (d) Crescenzi, R.; Solari, E.; Floriani, C.; Chiesi-Villa, A.; Rizzoli, C. *J. Am. Chem. Soc.* **1999**, *121*, 1695−1706. (e) Bachmann, J.; Nocera, D. G. *J. Am. Chem. Soc.* **2004**, *126*, 2829−2837. (f) Bachmann, J.; Nocera, D. G. *J. Am. Chem. Soc.* **2005**, *127*, 4730−4743.

(25) De Bruin, B.; Bill, E.; Bothe, E.; Weyhermüller, T.; Wieghardt, K. *Inorg. Chem.* **2000**, *39*, 2936−2947.

(26) Yang, X.-J.; Fan. X.; Zhao, Y.; Wang, X.; Liu, B.; Su. J.-H.; Dong, Q.; Xu, M.; Wu, B. *Organometallics*. DOI: 10.1021/om4003686.

(27) Szigethy, G.; Shaffer, D. W.; Heyduk, A. F. *Inorg. Chem.* **2012**, *51*, 12606−12618.

(28) Kaim, W.; Schwederski, B. *Pure App. Chem.* **2004**, *76*, 351−364.

(29) Sazama, G. T.; Betley, T. A. *Inorg. Chem.* **2010**, *49*, 2512−2524.

(30) King, E. R.; Betley, T. A. *J. Am. Chem. Soc.* **2009**, *131*, 14374−14380.

(31) Miller, J. B. *J. Org. Chem.* **1959**, *24*, 560−561.

(32) Murata, S.; Abe, S.; Tomioka, H. *J. Org. Chem.* **1997**, *62*, 3055−3061.

(33) Smith, P. A. S.; Hall, J. H. *J. Am. Chem. Soc.* **1962**, *84*, 480−485.

(34) Sazama, G. T.; Betley, T. A. *Organometallics* **2011**, *30*, 4315−4319.

(35) Bain, G. A.; Berry, J. F. *J. Chem. Educ.* **2008**, *85*, 532−536.

(36) Shores, M. P.; Sokol, J. J.; Long, J. R. *J. Am. Chem. Soc.* **2002**, *124*, 2279−2292.

(37) *Apex II*. Bruker AXS: Madison, WI, 2009.

(38) Sheldrick, G. M. *Acta Crystallogr., Sect. A: Found. Crystallogr.* **2008**, *64*, 112−122.

(39) Detailed crystallographic information can be found in the cif file (Supporting Information).

(40) Frisch, M. J.; Trucks, G. W.; Schlegel, H. B.; Scuseria, G. E.; Robb, M. A.; Cheeseman, J. R.; Scalmani, G.; Barone, V.; Mennucci, B.; Petersson, G. A.; Nakatsuji, H.; Caricato, M.; Li, X.; Hratchian, H. P.; Izmaylov, A. F.; Bloino, J.; Zheng, G.; Sonnenberg, J. L.; Hada, M.; Ehara, M.; Toyota, K.; Fukuda, R.; Hasegawa, J.; Ishida, M.; Nakajima, T.; Honda, Y.; Kitao, O.; Nakai, H.; Vreven, T.; Montgomery, Jr., J. A.; Peralta, J. E.; Ogliaro, F.; Bearpark, M.; Heyd, J. J.; Brothers, E.; Kudin, K. N.; Staroverov, V. N.; Kobayashi, R.; Normand, J.; Raghavachari, K.; Rendell, A.; Burant, J. C.; Iyengar, S. S.; Tomasi, J.; Cossi, M.; Rega, N.; Millam, J. M.; Klene, M.; Knox, J. E.; Cross, J. B.; Bakken, V.; Adamo, C.; Jaramillo, J.; Gomperts, R.; Stratmann, R. E.; Yazyev, O.; Austin, A. J.; Cammi, R.; Pomelli, C.; Ochterski, J. W.; Martin, R. L.; Morokuma, K.; Zakrzewski, V. G.; Voth, G. A.; Salvador, P.; Dannenberg, J. J.; Dapprich, S.; Daniels, A. D.; Farkas, Ö.; Foresman, J. B.; Ortiz, J. V.; Cioslowski, J.; Fox, D. J. *Gaussian 09*, Revision A.1; Gaussian, Inc.: Wallingford, CT, 2009.
(41) Neese, F. *ORCA—An ab initio, Density Functional and Semi-empirical Electronic Structure Package*, Version 2.7-00 ed.; Universität Bonn: Bonn, Germany, 2009.
(42) (a) Becke, A. D. *Phys. Rev. A* **1988**, *38*, 3098−3100. (b) Perdew, J. P. *Phys. Rev. B* **1986**, *33*, 8822−8824.
(43) Zhao, Y.; Schultz, N. E.; Truhlar, D. G. *J. Chem. Theory and Comput.* **2006**, *2*, 364−382.
(44) Schäfer, A.; Huber, C.; Ahlrichs, R. *J. Chem. Phys.* **1994**, *100*, 5829−5835.
(45) Schäfer, A.; Horn, H.; Ahlrichs, R. *J. Chem. Phys.* **1992**, *97*, 2571−2577.
(46) (a) Weigend, F.; Ahlrichs, R. *Phys. Chem. Chem. Phys.* **2005**, *7*, 3297−3305. (b) Weigend, F. *Phys. Chem. Chem. Phys.* **2006**, *8*, 1057−1065.
(47) (a) King, E. R.; Hennessy, E. T.; Betley, T. A. *J. Am. Chem. Soc.* **2011**, *133*, 4917−4923. (b) Römelt, M.; Ye, S.; Neese, F. *Inorg. Chem.* **2009**, *48*, 784−785.
(48) (a) Becke, A. D. *J. Chem. Phys.* **1993**, *98*, 5648−5653. (b) Lee, C. T.; Yang, W. T.; Parr, R. G. *Phys Rev. B* **1988**, *33*, 785−789.
(49) Neese, F. *Inorg. Chim. Acta* **2002**, *337*, 181−192.
(50) Neese, F.; Wennmohs, F.; Hansen, A.; Becker, U. *Chem. Phys.* **2009**, *356*, 98−109.
(51) Soda, T.; Kitagawa, Y.; Onishi, T.; Takano, Y.; Shigeta, Y.; Nagao, H.; Yoshioka, Y.; Yamaguchi, K. *Chem. Phys. Lett.* **2000**, *319*, 223−230.
(52) Neese, F. *J. Phys. Chem. Solids* **2004**, *65*, 781−785.
(53) Bencini, A.; Gatteschi, D. *J. Am. Chem. Soc.* **1986**, *108*, 5763−5771.
(54) Humphrey, W.; Dalke, A.; Schulten, K. *J. Mol. Graphics* **1996**, *14*, 33−38.
(55) *Persistence of Vision Pty. Ltd.*; Persistence of Vision (TM) Raytracer: Williamstown, Victoria, Australia, 2004. http://www.povray.org/.
(56) Antonello, S.; Musumeci, M.; Wayner, D. D. M.; Maran, F. *J. Am. Chem. Soc.* **1997**, *119*, 9541−9549.
(57) McMillen, D. F.; Golden, D. M. *Annu. Rev. Phys. Chem.* **1982**, *33*, 493−532.
(58) Eckert, N. A; Smith, J. M.; Lachicotte, R. J.; Holland, P. L. *Inorg. Chem.* **2004**, *43*, 3306−3321.
(59) Brown, S. D.; Peters, J. C. *J. Am. Chem. Soc.* **2004**, *126*, 4538−4539.
(60) Mankad, N. P.; Peters, J. C. *Chem. Commun.* **2008**, 1061−1062.
(61) Herrmann, W. A.; Kriechbaum, G.; Ziegler, M. L.; Wüknitz, P. *Chem. Ber.* **1981**, *114*, 276−284.
(62) Bart, S. C.; Bowman, A. C.; Lobkovsky, E.; Chirik, P. J. *J. Am. Chem. Soc.* **2007**, *129*, 7212−7213.
(63) (a) Ketterer, N. A; Fan, H.; Blackmore, K. J.; Yang, X.; Ziller, J. W.; Baik, M.-H.; Heyduk, A. F. *J. Am. Chem. Soc.* **2008**, *130*, 4364−4374. (b) Balch, A. L.; Holm, R. H. *J. Am. Chem. Soc.* **1966**, *88*, 5201−5209. (c) Warren, L. F. *Inorg. Chem.* **1977**, *16*, 2814−2819. (d) Anillo, A.; Diaz, M. R.; Garcia-Granda, S.; Obeso-Rosete, R.; Galindo, A.; Ienco, A.; Mealli, C. *Organometallics* **2004**, *23*, 471−481. (e) Bill, E.; Bothe, E.; Chaudhuri, P.; Chlopek, K.; Herebian, K.; Kokatam, S.; Ray, K.; Weyhermüller, T.; Neese, F.; Wieghardt, K. *Chem.—Eur. J.* **2005**, *11*, 204−224. (f) Chlopek, K.; Bill, E.; Weyhermüller, T.; Wieghardt, K. *Inorg. Chem.* **2005**, *44*, 7087−7098.
(64) (a) Nasri, H.; Ellison, M. K.; Krebs, C.; Huynh, B. H.; Scheidt, W. R. *J. Am. Chem. Soc.* **2000**, *122*, 10795−10804. (b) Nasri, H.; Ellison, M. K.; Shaevitz, B.; Gupta, G. P; Scheidt, W. R. *Inorg. Chem.* **2006**, *45*, 5284−5290.
(65) Hendrich, M. P.; Gunderson, W.; Behan, R. K.; Green, M. T.; Mehn, M. P.; Betley, T. A.; Lu, C. C.; Peters, J. C. *Proc. Nat. Acad. Sci. U. S. A.* **2006**, *103*, 17107−17112.
(66) Sinnecker, S.; Slep, L. D.; Bill, E.; Neese, F. *Inorg. Chem.* **2005**, *44*, 2245−2254.
(67) (a) Kharasch, M. S.; Sosnovsky, G. *J. Am. Chem. Soc.* **1958**, *80*, 756. (b) Kharasch, M. S.; Sosnovsky, G.; Yang, N. C. *J. Am. Chem. Soc.* **1959**, *81*, 5819−5824. (c) Rawlinson, D. J.; Sosnovsky, G. *Synthesis* **1972**, *1972* (1), 1−28. (d) Eames, J.; Watkinson, M. *Angew. Chem., Int. Ed.* **2001**, *40*, 3567−3571. (e) Andrus, M. B.; Lashley, J. C. *Tetrahedron.* **2002**, *58*, 845−866. (f) Gephart, R. T.; McMullin, C. L.; Sapiezynski, N. G.; Jang, E. S.; Aguila, M. J. B.; Cundari, T. R.; Warren, T. H. *J. Am. Chem. Soc.* **2012**, *134*, 17350−17353.
(68) (a) Jensen, M. P.; Mehn, M. P.; Que, L., Jr. *Angew. Chem., Int. Ed.* **2003**, *42*, 4357−4360. (b) Lucas, R. L.; Powell, D. R.; Borovik, A. S. *J. Am. Chem. Soc.* **2005**, *127*, 11596−11597. (c) Shay, D. T.; Yap, G. P. A.; Zakharov, L. N.; Rheingold, A. L.; Theopold, K. H. *Angew. Chem., Int. Ed.* **2005**, *44*, 1508−1510. (d) King, E. R.; Betley, T. A. *Inorg. Chem.* **2009**, *48*, 2361−2363. (e) King, E. R.; Sazama, G. T.; Betley, T. A. *J. Am. Chem. Soc.* **2012**, *134*, 17858−17861.
(69) (a) Dartiguenave, M.; Joëlle Menu, M.; Deydier, E.; Siebald, H. *Coord. Chem. Rev.* **1998**, *178−180*, 623−663. (b) Hillhouse, G. L.; Haymore, B. L. *J. Am. Chem. Soc.* **1982**, *104*, 1537−1548. (c) Mizobe, Y.; Ishii, Y.; Hidai, M. *Coord. Chem. Rev.* **1995**, *139*, 281−311. (d) Jenkins, D. M.; Betley, T. A.; Peters, J. C. *J. Am. Chem. Soc.* **2002**, *124*, 11238−11239.
(70) Weisser, J. T.; Nilges, M. J.; Sever, M. J.; Wilker, J. J. *Inorg. Chem.* **2006**, *45*, 7736−7747.
(71) Wallickt, E.; Cox, D. D.; Benkovic, S. J.; Bloom, L. M.; Bradley, F. C.; Nelson, M. J.; Que, L.; Wallick, D. E. *J. Am. Chem. Soc.* **1988**, *110*, 2026−2032.
(72) MacBeth, C. E.; Gupta, R.; Mitchell-Koch, K. R.; Young, V. G.; Lushington, G. H.; Thompson, W. H.; Hendrich, M. P.; Borovik, A. S. *J. Am. Chem. Soc.* **2004**, *126*, 2556−2567.
(73) DiFranco, S. A.; Maciulis, N. A.; Staples, R. J.; Batrice, R. J.; Odom, A. L. *Inorg. Chem.* **2012**, *51*, 1187−1200.